

Three-Dimensional Urban EM Wave Propagation Model for Radio Network Planning and Optimization Over Large Areas

Yoann Corre and Yves Lostanlen, *Member, IEEE*

Abstract—A new 3-D urban electromagnetic wave propagation model is presented. It provides fast 3-D deterministic predictions in urban radio configurations and over large areas. The various techniques to make it suitable to the network planning and optimization of large wireless networks are described. The resulting radio propagation maps exhibit seamless coverage between the various environments (dense urban, urban, and suburban). The model efficiently addresses all types of outdoor transmitter configurations (macrocells, minicells, microcells, and picocells) and all types of receiver locations (at ground level, over the rooftop, and at high building floors). It predicts the field strength as well as the dominant specular contributions of the impulse responses to build ray spectra (including delays and angles). Thus, the model may also be used to estimate the performances of new radio systems [diversity and multiple-input–multiple-output (MIMO)]. The narrowband power prediction of the model is evaluated by comparison with microcell measurements. The evaluation stresses the advantage of 3-D modeling compared with the vertical-plane approach or 2-D ray tracing. Finally, the ability of the model to simulate radio wideband characteristics in a complex environment is demonstrated by comparing delay-spread estimates to measurements collected from a high-macrocell transmitter in a hilly city and to arrival angles collected in a suburban macrocell area.

Index Terms—Radio network optimization, radio network planning, ray tracing, urban environment.

I. INTRODUCTION

NEW RADIO networks, such as third-generation (3G), beyond 3G (B3G), and fourth-generation (4G), involve complex air interfaces that require advanced simulation tools for each layer of the system: first, for the design of standards and, second, for the planning and optimization of radio access networks. In particular, sophisticated techniques like diversity or multiple input–multiple output (MIMO), which are employed in various environments and for different kinds of transmitter–receiver configurations, permit the air interfaces to take advantage of the multipath radio channels. In addition, the air interface of code-division multiple-access (CDMA) networks has a frequency reuse of 1. The system is, therefore,

interference limited, and the coverage and the capacity are linked together [1]. The prediction of the serving cell limits, the soft handover areas, and the determination of interference boundaries need to thoroughly be defined in the dense 3G network. Only an accurate propagation model can be used to estimate these coverages, because they set the fundamental limits of dimensioning, planning, and optimization of the 3G networks [2]. Furthermore, new interfaces based on orthogonal frequency-division multiplexing (OFDM) offer adaptive modulation and coding in 3G long-term evolution (LTE) [3], ultramobile broadband (UMB) [4], worldwide interoperability for microwave access (WiMAX) [5], [6], and digital video broadcasting-terrestrial (DVB-T) [7]. A hierarchical mode is also specified in DVB-T [8]. This means that the possible served bit rates will depend on the area where the receivers are located and indirectly on the reception levels. To finely anticipate the capacity of the former system and the coverage of both techniques, an accurate propagation model is mandatory.

Digital television (fixed or mobile) usually involves high tower sites complemented by gap fillers embedded in the cities to extend the coverage. To get a reliable coverage for the whole network, the propagation prediction techniques should provide seamless coverage from the high towers (usually macrocell in rural or suburban areas) down to dense urban areas, where the gap fillers are inserted in a minicellular or even street-level configuration. Clearly, the new networks, which are based on recent air interfaces, require propagation prediction with a high dynamic range of reception levels to determine the useful service coverage areas for various transmitter antenna heights and over large areas.

Many propagation prediction techniques have been proposed over the last decade [9]–[12]. Ray models generate a high interest, as they succeed in predicting with high accuracy the field strength around low transmitters in urban environments. For very low transmitter heights, the propagation is confined between the buildings, and thus, the first approaches were mainly 2-D (horizontal plane) [9], [13], [14]. The 3-D ray-tracing models (or similar techniques) are good candidates to estimate the site-specific space–time characteristics of the narrowband or wideband urban propagation channel, which are essential for the simulation of the performance of new radio systems [11]. In recent years, many works have presented comparisons of multipath predictions to wideband channel characteristics, such as the power delay profile (PDP), the delay spread, or the angular spread [15], [16]. These techniques are consequently useful and reliable to deterministically assess the wideband radio channel.

Manuscript received March 31, 2008; revised October 6, 2008. First published March 6, 2009; current version published August 14, 2009. This work was supported in part by the “Agence Nationale de la Recherche.” The review of this paper was coordinated by Prof. S. K. Chaudhuri.

Y. Corre is with Siradel, 35043 Rennes Cedex, France (e-mail: ycorre@siradel.com).

Y. Lostanlen is with Siradel, Toronto, ON M4S 3E2, Canada (e-mail: yves.lostanlen@ieee.org).

Color versions of one or more of the figures in this paper are available online at <http://ieeexplore.ieee.org>.

Digital Object Identifier 10.1109/TVT.2009.2016973

These prediction methods rely on geographical map data that require high-resolution (HR) accuracy and an adaptation to the propagation problem (e.g., limiting the number of useless diffracting edges, internal courts, and vertical details). These kinds of accurate geographical map data may be expensive.

However, the main restrictive aspect of 3-D ray tracing for large usage in radio planning generally remains the CPU time. Some techniques have recently been elaborated upon and are the subject of continuous work to speed up the computation, particularly for coverage computation. When the 3-D ray tracing is based on computer image theory, the acceleration techniques generally involve a preprocessing of the vector database [17], [18] and extract the main geometrical and physically meaningful elements, which leads to the computation of the field strength. Often, the simplifications are efficient in terms of computation time, but they result in the prediction of only dominant paths that may be dependent on transmitter site characteristic. For areas corresponding to the usual small 3G cell radius, these propagation models give satisfying coverage results.

Another way to optimize the computation times consists of mixing ray launching and ray tracing [15], [19], which are separated in two planes (vertical and horizontal). The approach considering the propagation first in the horizontal plane and then in the vertical plane creates a small error on the trajectory of the rays diffracted by the horizontal edge of buildings, but comparisons of the predictions to measurements give a very good agreement.

More recently, in the frame of a European Project Momentum, [20] and [21] suggested a progressive propagation “city model” that is decomposed into three main steps: vertical plane (knife-edge diffraction over building), multipath (single scattering processes considering Lambertian transmitters), and vegetation models (for all paths).

The 3-D urban model presented in this paper is an alternative to most quoted models that gather the main advantages of each solution. The focus is set on the operational use of these propagation models for radio network planning and optimization over large areas.

The rest of this paper is organized as follows. Section II describes the basic concept of the model considering propagation in the horizontal and vertical planes in two different stages. In the first stage, the 2-D ray-launching technique constructs the horizontal trajectory of the rays. A homogeneous ray density is obtained all over the computation area (whatever the distance from the transmitter) by launching rays on all building walls and with an adaptive beamwidth. Another strength of 2-D ray launching is the elaboration of a visibility mask (VM) after each interaction (reflection, diffraction, indoor penetration, or interaction above a building podium) to determine the area where the rays may catch the receivers but also further interactions with the building walls, which results in computation time savings. Then, in the second stage, the determination of the main obstacles in the ray vertical plane simulates propagation from an infinite number of diffractions. It combines the uniform theory of diffraction (UTD) and a modified Deygout method to compute the field strength of the 3-D rays. The computation times are much lower than those of the full 3-D ray-tracing methods. This is the key point for an operational use for

the radio planning and optimization works. Section III presents some enhancements for adapting the model to predictions over large areas. The described 3-D urban model divides the coverage area into a “near-reception region,” where all ray contributions are computed, and a “far-reception region,” where only the dominant contributions that propagate over rooftops are predicted. This method efficiently reduces the computation times and offers a seamless transition between large operational regions represented by both HR and low-resolution (LR) geographical map data. Moreover, the heterogeneous geographical map data are inherently managed, as the algorithm computing the diffraction in the vertical plane handles data coming from distinct resolutions or distinct formats (vectors or raster). All these characteristics, combined with other characteristics explained in the remainder of this paper, make the 3-D urban model convenient for expert usage, e.g., prediction of a picocell, but also and above all for large-scale planning and optimization of urban radio cellular and broadcast systems. Section IV evaluates the performance of the described model by comparison to microcellular power measurements and to macrocellular measurements with high delay or angular dispersion. Finally, Section V illustrates the application of the described model for the prediction of a large urban coverage from a heterogeneous geographical map data.

II. 3-D URBAN MODEL DESCRIPTION

This section describes in detail the algorithm of the 3-D urban model, referring frequently to Fig. 1, where the basic concept is depicted.

The 3-D urban model needs an HR representation of the transmitter environment given in the digital geographical map data: terrain altitude (in a pixel grid, so-called raster matrix), 3-D building contour vectors, and optionally a representation of additional clutter types (other than buildings) in raster matrices or vectors. The HR representation can be completed with LR data for predicting the propagation to the surrounding suburban or rural environments. The LR data are composed of raster matrices that only provide a rough statistical description of the clutter, with no precise contour or clutter height. Fig. 2 shows an example from an HR dense urban European environment. The transmitter shown in this example is used in the remainder of the paper to illustrate the model algorithm. It is located on a 3-m mast above the roof of a 22-m-high building. The surrounding buildings are in average higher than 25 m, i.e., above the transmit antenna. Thus, the transmit antenna is considered to be “embedded” in the city, presenting a difficult configuration for the propagation prediction. The techniques described in the following sections explain how the 3-D urban model can cope with such a situation.

A. Computing the Direct Contribution in the Vertical Plane

The first step of the algorithm (see Fig. 1) consists of simulating the direct-path contribution for all the receiver positions. The so-called “direct path” is the path linking the transmitter and the receiver, possibly interacting with the obstacles located in the vertical plane, including both terminals.

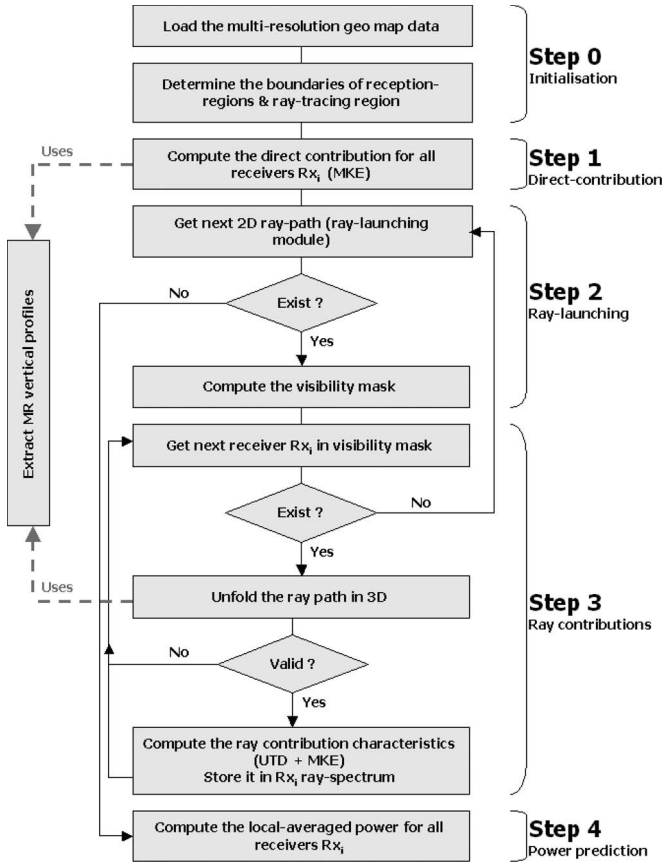


Fig. 1. Flowchart of the 3-D urban model.

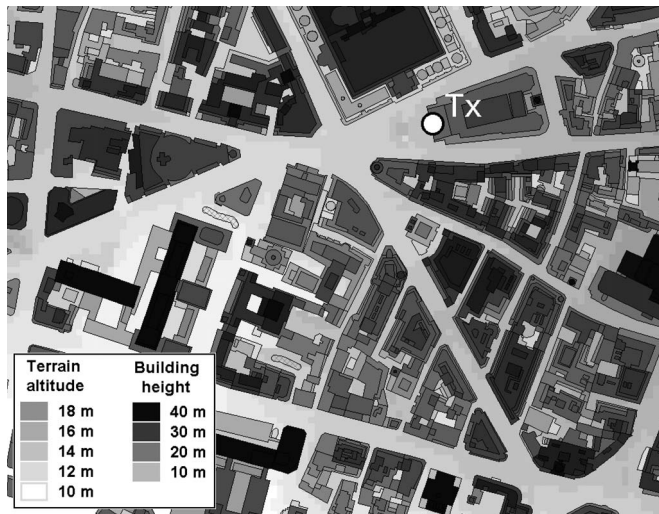


Fig. 2. Small macrocell transmitter (22 m high) within the HR geographical map data.

The estimation of the radio wave propagation over an irregular terrain considers the main obstacles placed between the transmitter and the receiver as “equivalent” knife edges. Approximates of the multiple knife-edge (MKE) diffraction give quite simple solutions and are widely used in rural areas [22]. The presented approach adapts the MKE methods to predict the over-rooftop diffraction in urban areas [23]. The adaptation mainly lies on the selection method of the diffraction edges and

on the thresholding applied on the diffraction values estimated by large urban measurement campaigns. In this environment, the obstacles giving rise to diffraction phenomena are basically the trees, the building rooftops, and the terrain obstructions.

The direct-path prediction achieves a high accuracy when using rigorous digital representations of the geographical urban zones. However, a strength of the proposed method is the smooth transition for predictions based on HR to LR geographical map data. This provides a coherent and homogeneous propagation model for dense urban, urban, and suburban areas by allowing a seamless coverage between these areas. This is a key advantage over existing methods, i.e., making use of UTD in the vertical plane or using street characteristics (width, orientation, etc.) [24]–[26].

The exploitation of only the direct path in the urban environment suffers from critical limitations. Indeed, the computed contributions are in the forward direction between the transmitter and the receiver, which is not sufficient to properly describe the propagation for antennas embedded in the city. The interactions on building facades in the vicinity of the radio link, which cause multi path components, are not taken into account.

B. Lateral Ray Construction

The second step of the algorithm, i.e., the ray-launching step (see Fig. 1), consists of the construction of 2-D horizontal ray paths from specular reflections on building facades and diffractions on building vertical edges. The ray-path construction is based on a launching technique that proved to be more efficient in terms of computation times than the usual image theory when simulating over large reception areas.

On one hand, ray tracing based on the image theory calculates the accurate trajectory of reflected and diffracted paths between specific transmitter and receiver positions [27]. The geometrical construction is accurate, but the computation times are a serious drawback. They are proportional to the number of receivers, and overall, they exponentially increase with regard to the number of building segments in the computation area and to the maximum interaction order (i.e., the maximum number of interactions along a ray).

On the other hand, the ray-launching technique consists of launching a set of ray beams with (usually) a uniform angular width around the transmitter and diffracting edges. The horizontal propagation space is sampled. The ray path at the center of these ray beams propagates along straight lines in the open areas and undergoes reflections or diffractions when reaching a building contour. Then, a full transmitter–receiver ray is constructed if the ray beam catches a receiver. The computation times still exponentially increase with regard to the maximum diffraction order, but they only proportionally increase to the number of receivers, the number of building segments in the computation area, and the maximum reflection order. These characteristics make the ray launching time efficient for coverage predictions, whereas the approximations due to space sampling reduce the accuracy.

The technique implemented in the presented 3-D urban model computes various categories of 2-D horizontal rays that

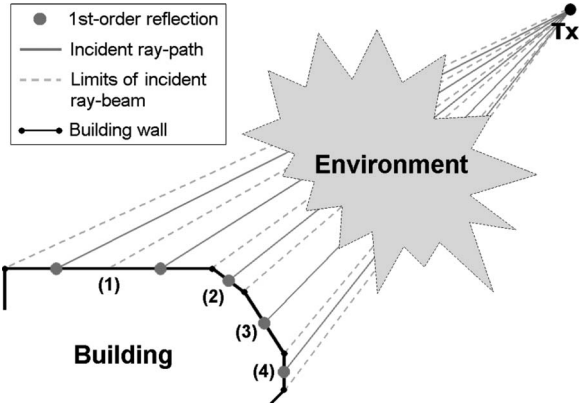


Fig. 3. Nonuniform launching to the first-order reflection points. Two reflection points are created on wall (1), whereas one single reflection point is created at the center of walls (2)–(4).

are all referred to as “T-A-nR-qD-mR-sI” rays, where “T” stands for “transmitter,” “A” for “above building rooftops,” “R” for “reflection,” “D” for “diffraction,” “n” is the number of reflections before diffraction, “q” is the number of diffractions (0–2), “m” is the number of reflections after diffraction, and “s” is the number of indoor penetration (0 or 1). The proposed model combines some original techniques, such as the nonuniform angular beamwidth and the construction of VMs, which are detailed hereafter.

Proposed Ray-Launching: First, T-A-1R rays are launched from the transmitter toward all the exterior building contours to generate first-order reflections. As illustrated in Fig. 3, the obstacles between the transmitter and the first-order reflection are not taken into consideration at this stage, as the propagation above these obstacles will be managed later in the analysis of the unfolded ray profile (see Section II-A). Then, the reflected ray path is constructed in the specular direction of the reflection, according to the Fermat principle.

The angle between two adjacent T-A-1R rays is not constant. The ray launching finds all first-order reflected paths between the transmitter and the receivers. At least one T-A-1R ray is launched on each building wall oriented toward the transmitter, whatever the size of the wall or the distance from the transmitter. As shown in Fig. 3, the ray beam is necessarily limited by the edges of the wall. Using this simple method to create only one T-A-1R ray per wall proved to be sufficient to get accurate predictions of the narrowband power when using detailed geographical map data (i.e., with short building walls). The method is further enhanced by the introduction of the maximum angular step θ_{STEP} and the maximum linear step d_{STEP} to restrict the width of the ray beam when the wall is large. This restriction corresponds to a division of the ray-beam launched to a wall, reducing the approximations on the position of higher order reflections when rays are launched close to the transmitter (impact of θ_{STEP}) or at large ranges (impact of d_{STEP}). To clarify the principle, let us consider a building wall with edge points P_1 and P_2 separated by a distance d . The angular distance between both edge points, as seen from the transmitter, is $\theta = \|\arccos(\vec{u}_1 \cdot \vec{u}_2)\|$, where \vec{u}_1 (respectively, \vec{u}_2) is the 2-D unit direction vector from the transmitter to the first edge P_1 (respectively, to the second edge P_2).

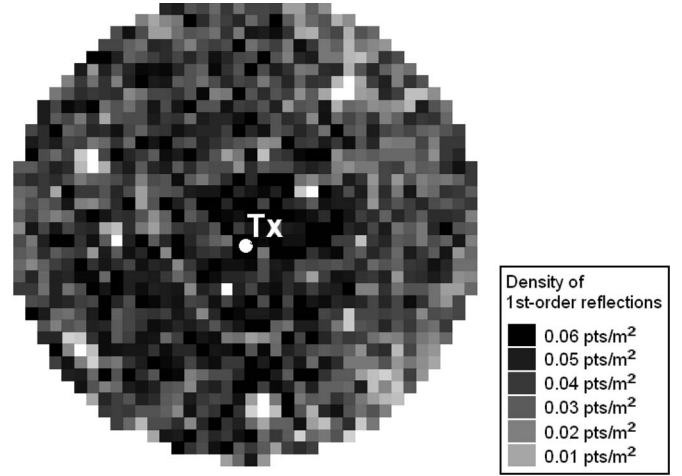


Fig. 4. Density of first-order reflections around the transmitter.

The number of first-order reflections on the building wall is then given by

$$n = \left(\max \left(\frac{d}{d_{\text{STEP}}}; \frac{\theta}{\theta_{\text{STEP}}} \right) \right)^+ \quad (1)$$

where the operation $(\dots)^+$ consists of taking the larger or equal integer value. The ray beamwidth is $\theta_{\text{RAY}} = \theta \div n$.

Finally, the density of first-order reflections is roughly homogeneous over the computation areas, where the building distribution is constant. This is illustrated in Fig. 4, where $\theta_{\text{STEP}} = 4^\circ$, and $d_{\text{STEP}} = 4$ m.

T-A-1D rays are launched as well from the transmitter on all the building edges oriented toward the transmitter. Here, again, the obstacles between the transmitter and the diffraction edge are not taken into consideration; the rays are launched over the whole computation area.

VM: Using a “reception sphere” is a common technique to determine when a ray beam catches a receiver [9]. The ray path (at the center of the ray beam) must intercept a sphere that is centered on the receiver, the radius of which is equal to the ray half-beamwidth. Then, a test checks that no building obstruction occurs between the receiver and the last interaction of the ray beam.

In the proposed 3-D urban model, the construction of the VM advantageously replaces the “reception sphere” technique. The VM contains the whole 2-D area that can be reached by the ray beam after reflection, diffraction, or indoor penetration. As shown in Fig. 5, the reflection VM (VM of a reflected ray) is limited on one side by the reflecting wall and on the other side by the portions of building walls that obstruct the ray beam. In a similar way, the diffraction VM (VM of a diffracted ray) is composed of all portions of the building walls that are visible from the diffraction edge. In the following, “VM walls” refer to the portions of building walls that compose the VM boundaries.

The VM construction permits the rapid execution of five different operations. The primary goal is the rapid detection of all receivers caught by the ray beam. As the receivers are generally distributed over a pixel grid (for coverage predictions), the detection consists of searching for adjacent and regularly

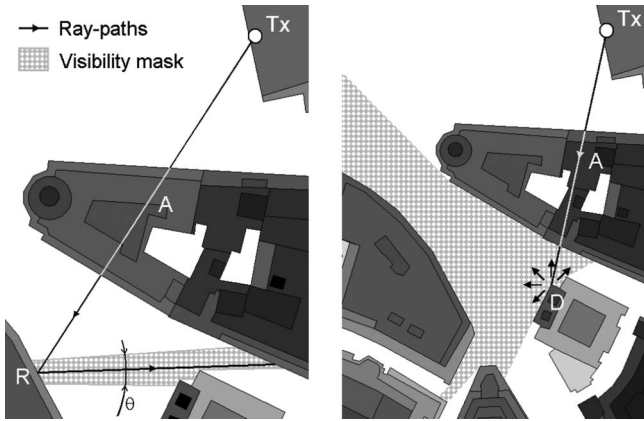


Fig. 5. VM of (left) a reflected and (right) a diffracted ray path.

spaced pixels contained in a closed polygon formed by the VM boundaries. A time-efficient geometric analysis is done, and no obstruction test is necessary. This replaces the “reception-sphere” method and is specially suited when computing HR pixel grids (e.g., 5 m).

In addition to this primary goal, VM is used for the rapid determination of the higher order reflection points. In the case of a reflection VM, the higher order reflection point is the intersection between the reflected ray path and the VM walls. In the case of a diffraction VM, the higher order reflection points are found by directly launching rays to VM walls.

In addition, the identification of the diffraction edges in T-A-nR-D rays requires no additional computation time. They simply correspond to the edges of the VM walls (only the ones being real building edges).

Similarly, the indoor penetration walls used in the construction of outdoor-to-indoor ray paths simply correspond to the VM walls.

Finally, the last operation where VM is involved is the construction of the interactions on far obstacles, as explained later in Section III.

The configuration stressed in Fig. 6 (by the arrow) requires the elaboration of an adapted VM. This configuration, where the first-order reflection occurs on the wall of a podium building, is regularly met in very dense urban areas as Manhattan (New York City) or Hong Kong. In that case, the building walls obstructing the VM are only searched after the reflected ray path reaches the open area (then not just after the reflection position). Thus, the rays reflected on the podium buildings can propagate back in the streets, allowing for the construction of rays reflecting on podium buildings.

Higher Order Interactions: Higher order reflections are generated in T-A-nR rays until the ray reaches the maximum number of allowed reflections or reaches the boundary of the computation area.

Rays with a diffraction occurring after n reflections or after one diffraction, i.e., T-A-nR-D or T-A-2D, are constructed from the diffraction on building edges detected in the incident ray-path VM.

The construction of reflections after diffraction is possible when simulating a rich impulse response. This kind of ray provides important contributions for the estimate of the space-time

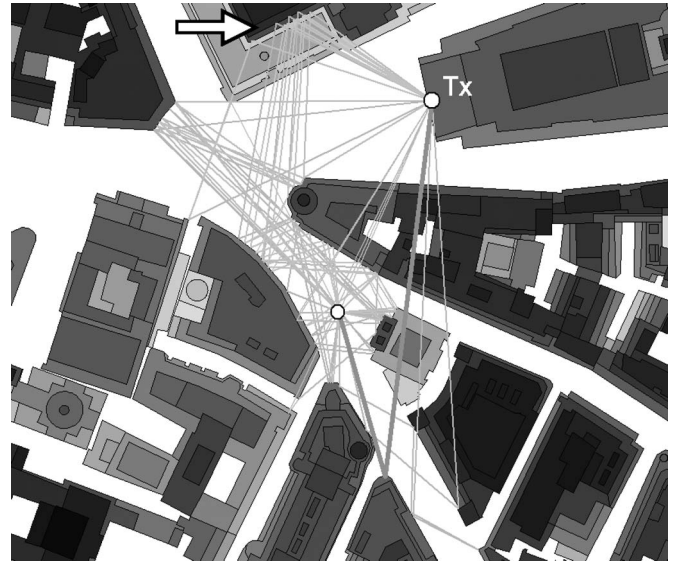


Fig. 6. Three-dimensional ray contributions from the small macrocell transmitter to a street-level receiver position.

characteristics of the propagation channel; however, in most cases, their impact on the total received power can be neglected, whereas the required computation is time expensive. The T-A-D-mR or T-A-nR-D-mR rays are constructed in a way similar to the T-A-nR rays, except that the reflections are only positioned on the portions of building walls that compose the diffraction VM. Successive reflected ray paths are constructed until the ray reaches the maximum allowed number of reflections (adding the n reflections before diffraction and the m reflections after) or the boundary of the computation area.

Finally, indoor penetration is computed to simulate the coverage inside buildings. All the outdoor ray paths are prolonged through the building walls that compose the incident ray-path VM and then along a straight line inside the building [11, pp. 137–138].

C. Unfolding the Ray Paths in 3-D

The calculation of the 3-D ray trajectory after a 2-D ray catches a receiver takes place in the third step of the algorithm (see Fig. 1).

The 3-D trajectory is realized by gathering the vertical terrain profile of each ray path into an “unfolded profile” that gives the variations of the ground altitude, clutter type, and clutter height from the transmitter to the receiver, as shown in Fig. 7. Another key point of the method toward a homogeneous propagation model lies in the fact that the same MKE diffraction method is applied on the direct path and on this “unfolded profile” to detect the main obstacles and compute a diffraction loss.

The effect of vegetation in the “unfolded profile” is essential. This effect can be approximated by a knife-edge diffraction on top of the vegetation and a transmission through the vegetation block [20]. However, the calculation of transmission loss cannot be accurate when using the propagation model for large-scale radio planning because of the lack of precision in the geographical map data (the width of tree rows is generally a rough estimation, the type of foliage is generally not specified) and

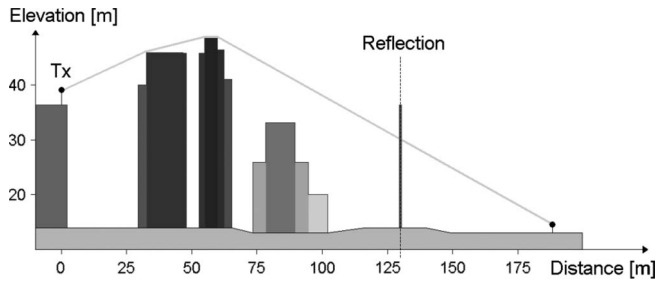


Fig. 7. Unfolded terrain profile along the ray path (corresponding to the thick 2-D path in Fig. 6).

because the loss calculation should be adapted to the season. Therefore, the 3-D urban model implements an approximate solution; first, a clearance of this land usage is operated around the receiver (e.g., 50 m clearance), and second, knife-edge diffraction is computed from the remaining vegetation.

At this stage, the algorithm calculates a kind of poly-line that represents the shortest path from the transmitter to the receiver passing over the main obstacles detected in the “unfolded profile.” This poly-line represents the ray trajectory in the vertical plane. If the trajectory goes below the ground level or above the interacting buildings (interaction found in the 2-D ray path), then the ray is not valid and rejected (see Fig. 1). There is an exception when the trajectory at the first-order reflection of a T-A-nR- ray is above the reflecting building, but the height difference is lower than a margin; then, the reflection is transformed into a back diffraction occurring at the building horizontal edge [19].

D. Computing the Ray Contributions

The field strength of the new ray contribution is calculated from a combination of the UTD and the MKE method. The calculation for one given linear polarization is expressed as

$$\|E\| = G_T \times (C_{MKE} \cdot C_{INDOOR} \cdot \|E_{UTD}\|) \times G_R \quad (2)$$

where $\|E\|$ is the received electromagnetic (EM) field strength in volts per meter, G_T is the transmit antenna gain, G_R is the receive antenna gain, C_{MKE} is the diffraction coefficient calculated from the MKE method taking into consideration only the propagation in the “unfolded profile,” C_{INDOOR} is the indoor propagation coefficient calculated from the in-building ray length, and $\|E_{UTD}\|$ is the received EM field strength in volts per meter calculated by UTD from the interactions of the horizontal 2-D ray path only, i.e., without considering the diffractions above the obstacles. All the terms in (2) are scalar values.

The transmit and receive antenna gains are generally extrapolated from the 2-D plane antenna patterns given in one specific polarization by the manufacturer. The extrapolated 3-D antenna gain is given from a sophisticated technique [28].

The UTD coefficients are calculated assuming that the propagation takes place in a quasi-horizontal plane. Thus, the building facades and the building edges are considered as surfaces or edges perpendicular to the propagation plane. The 2-D heuristic diffraction coefficient for dielectric materials proposed in [29]

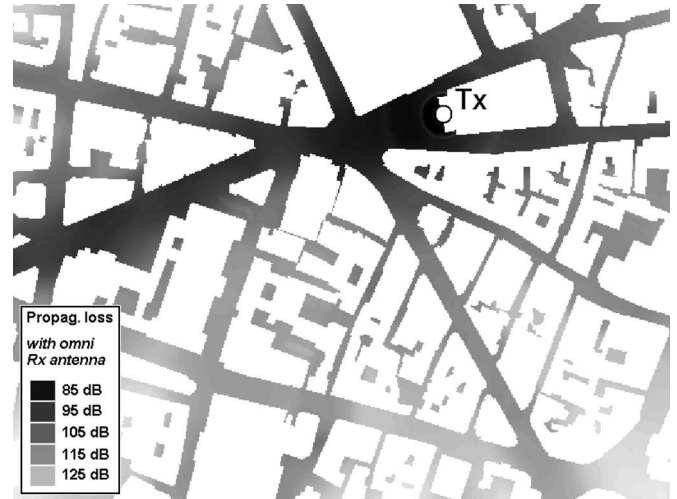


Fig. 8. Map of the predicted narrowband power.

and [30] and the double-diffraction coefficient proposed in [31] are used to calculate the coefficient from diffraction(s) on the building vertical edges.

The application of the 3-D UTD coefficient [29] for all interactions was analyzed, but the comparison to measurements did not show any significant improvement in the prediction of the narrowband power level, although the computation complexity was increased. The 3-D urban model does not calculate the complex field of the ray contribution but only the norm. The reason is that the phase error is likely to be larger than 2π due to inaccuracies in the geographical map data for common wavelengths used in radio networks. Moreover, the complex antenna gain is generally unknown, and the MKE method only provides an approximate of the diffraction loss as a scalar value. Thus, the phase of the ray contribution is not calculated and must be considered as a random variable uniformly distributed over the interval $0;2\pi$ rad. Then, the ray spectrum of the predicted receiver is enlarged, adding the ray contribution characterized by its norm, delay, angle of departure, and angle of arrival.

E. Computing the Prediction Result

In the last step of the simulation (see Fig. 1), the narrowband received power is obtained from the “incoherent” summation of ray fields, i.e., a norm square summation is made and not a vectorial summation. Fig. 8 presents an example where the narrowband received power is simulated over the computation area with 5-m-wide pixels.

Generally, in the process of planning and optimizing networks, the propagation maps must be predicted for different transmitters having the same location but not the same antenna characteristics (predicting sector transmitters or predicting various antenna orientations). The storage of the ray contributions during prediction afterward allows for fast and successive unmasking (removing antenna gains) and masking operations. An operational time-efficient prediction of all the collocated transmitters is obtained as the ray contributions are computed only once.

III. ENHANCEMENT FOR LARGE AREAS

The presented algorithm based on ray launching and VMs may be enhanced to support large-scale computations for huge metropolitan areas or even for national areas beyond urban areas.

A. Interaction With Far Obstacles

The ray contributions described in Section II propagate above the rooftops before they undergo interactions with the building facades and thus propagate along the streets. The interaction on the building facades generally occurs in the vicinity of the receiver position (a few hundreds of meters around). Thus, interactions on obstacles far away from the receiver are not predicted by the described ray contributions, although they can bring significant signal depending on the configuration. For example, when the transmitter antenna is located under the surrounding rooftops, then the building facades close to the transmitter create some strong contributions, propagating afterward above rooftops and possibly reaching far receivers. In addition, the interactions with unobstructed and far buildings (far from both the transmitter and the receiver) generate contributions with long delays that must be considered in the prediction of the radio link quality of service (QoS). These contributions directly impact the interference intersymbol or the downlink orthogonality factor in CDMA systems.

Some 2-D ray paths presented in Section II are also used to simulate contributions interacting with obstacles far away from the receiver; however, this process can be very time consuming, depending on the propagation environment. If the interaction of a T-A-1R or T-A-1D ray path is likely to be in line-of-sight (LOS) from the transmitter, then step 3 of the algorithm (see Fig. 1) searches in a conventional way for receivers within the VM, but additional receivers are also searched beyond the VM walls. The rays that reach these additional receiver positions propagate first above rooftops, interact with a building facade, and then propagate again above rooftops. After the construction of the 3-D trajectory, these rays are considered as valid only if the first interaction is really in the LOS of the transmitter.

Fig. 9 presents a study case in an urban environment, where the interactions on far obstacles are preponderant. The street-level receiver is more than 5 km away from a high macrocellular transmitter. The direct path is obstructed by a hill covered by high trees. However, the buildings located on the hills surrounding the receiver and in the LOS of the transmitter generate reflections and diffractions given contributions with field strength comparable with the direct contribution. Extra delays of up to 11 μs with significant strength can be observed in the predicted PDP. This result is validated below by comparison to measurements; the present study case corresponds to the measurement point 26 in Section IV-B.

B. Complements to Predict Large-Scale Coverage

As the 3-D urban model is dedicated to the calculation of large coverage maps for radio planning and optimization tasks, the model has to be fast and adapted to the multiresolution ge-

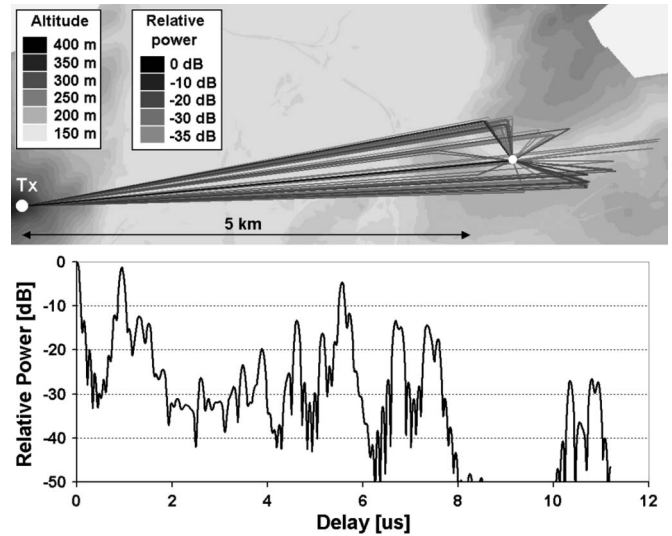


Fig. 9. Predicted PDP with interactions by far obstacles.

ographical map data that are generally used by radio planners, i.e., the HR data in some urban environments including 3-D building contours and the LR data elsewhere. The model fulfils these objectives by the implementation of two complementary solutions: the extraction of multiresolution vertical profiles and the division of the computation area into four different regions.

Composite Vertical Profile: The first technique to cope with large-scale computation is the multiresolution vertical profile. It represents the variations of terrain altitude, clutter types, and clutter heights between two points, with a step that is not necessarily uniform, and extracting the data from different kinds of sources, i.e., 3-D vectors, HR raster data, or LR raster data. This extraction is seamless and flexible: it automatically adapts to the data availability and obeys to preference settings (preference for vector or raster data) when different kinds of data are available in the same area. As an example, a vertical profile may be constructed from 3-D vector data and HR altitude data (as long as the path is located in the urban environment) and then from LR raster data for the portion of the path located outside the urban environment. As shown in Fig. 1, this vertical profile is constructed not only for the direct path but for the multipaths given by the ray-launching process detailed in Section II as well. The paths propagating in different areas represented by multiresolution geographical map data are predicted with seamless transitions.

Four Types of Region: The computation area is divided into several regions: three reception regions having different prediction characteristics, i.e., the categories of rays allowed to catch the receivers differ, and the ray-tracing region where the ray-launching interactions are allowed to occur. This division permits the computation of large coverage maps with competitive times, whereas multipaths having a preponderant impact on the narrowband power are still constructed.

In the near-reception region, all types of ray contributions are computed. Thus, the narrowband and wideband channel characteristics may be predicted there. In the far-reception region, only the direct-path T-A-1R-A and T-A-1D-A contributions are computed, allowing only for the computation of the narrowband

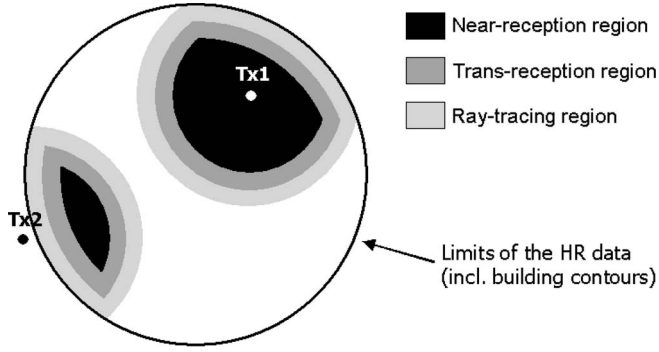


Fig. 10. Division of the computation area.

TABLE I
RULES TO DETERMINE THE RECEPTION REGION

Region	Rules
Near-reception	If $d_{T-R} < D_{NEAR}$ and $d_{R-V} > (L_{RT} + L_{TRANS})$
Trans-reception	Else if $d_{T-R} < (D_{NEAR} + L_{TRANS})$ and $d_{R-V} > L_{RT}$
Far-reception	Else

received power. Then, in the transition-reception region, the received power is the sum of the narrowband power calculated like in the near-reception region weighted by a coefficient ρ and the narrowband power calculated like in the far-reception region weighted by $1 - \rho$; the determination of ρ is shown in detail later. The division of the computation area is illustrated in Fig. 10. The far-reception region is not represented but is complementary to the near and transition regions.

The interactions of the 2-D rays are only constructed on the building walls located in the ray-tracing region. This region is the intersection between the HR geo map data and the disk of radius D_{RT} centered on the transmitter. It is larger than the transition region to allow the rays propagating slightly beyond the area where they catch the receivers.

Table I gives the rules to determine which reception region includes a given receiver. We note d_{T-R} as the distance between the transmitter and the receiver and d_{R-V} as the minimum distance between the limits of the vector data and the receiver. If the receiver is located within the vector data limits, then the distance d_{R-V} is positive. Elsewhere, the distance d_{R-V} is set to zero. D_{NEAR} is the radius of the near-reception region. L_{TRANS} is the length of the transition-reception region. L_{RT} is the extra length of the ray-tracing region such that $D_{RT} = D_{NEAR} + L_{TRANS} + L_{RT}$. Fig. 10 gives two examples. In the first example (on the top right side of the figure), the transmitter is included in the limits of the HR geographical map data. In the second example (bottom left), the transmitter is outside the limits of the HR data.

We found 500 m as the best tradeoff between computation time and accuracy for D_{NEAR} . This value, which is also observed in [20], is generally sufficient to predict the ray contributions that significantly impact the narrowband power.

The length L_{RT} of the transition-reception region is fixed to 100 m to guarantee a seamless transition between regions where the simulated propagation mechanisms differ. The weighting coefficient ρ is related to the propagation distance d_{T-R} and

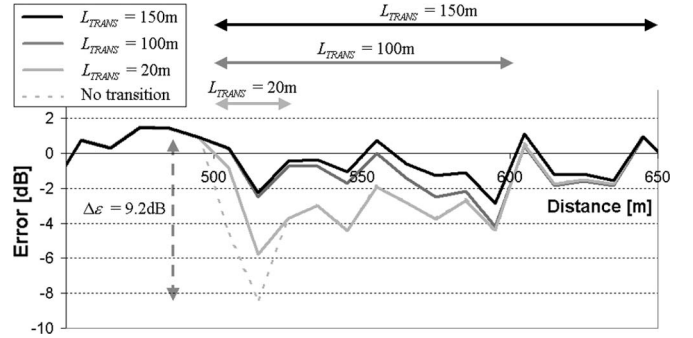


Fig. 11. Impact of the length of the transition region, where the near-reception region ends at a distance of 500 m.

to the distance d_{R-V} , linearly increasing from the beginning to the end of the transition-reception region, i.e.,

$$\rho = \min \left(\frac{D_{NEAR} + L_{TRANS} - d_{T-R}}{L_{TRANS}}, \frac{d_{R-V} - L_{RT}}{L_{TRANS}} \right). \quad (3)$$

Fig. 11 shows the impact of the length L_{RT} on prediction results in the transition-reception region. The prediction is compared with the power measurements collected in a dense urban environment around a small macrocell transmitter. Then, the mean of the prediction error is calculated for different propagation distances (over 10-m-wide intervals). The absence of transition results in a sharp drop of the mean prediction error at the end of the near-reception region, although a transition length larger than 100 m prevents any breaking. As the computation time increases with the transition length, $L_{RT} = 100$ m is a good tradeoff.

Finally, the presented division of the computation area results in a seamless transition between HR and LR geo map data, as the limits of the different regions depend on the limits of the vector data. That is an efficient way to automatically adapt the simulated propagation mechanisms to the available data. Thus, in the operational context, the radio planners can apply the same propagation model to all urban transmitters.

IV. PERFORMANCE EVALUATION

In a first example presented in this section, the performance of the 3-D urban model is evaluated by a comparison to drive-test power measurements in different urban environments. Two other propagation models are also evaluated: the vertical-plane model that only computes the direct path from the MKE method and the 2-D ray-tracing model that combines 2-D ray-tracing contributions in the horizontal plane and the MKE method for the direct path [23].

The second example analyzes the wideband prediction of the 3-D urban model that is compared with the delay-spread measurements collected in a wide urban and hilly environment. The interactions with far obstacles are allowed there and are necessary to get reliable results.

Finally, the last example compares predictions of the horizontal arrival angles to measurements collected at short propagation ranges in a suburban macrocell.

TABLE II
RESULTS FROM THE EVALUATION TEST

Model	RMS Error [dB]	Correlation
<i>Blind test (calibration from 11 measurements)</i>		
Vertical-Plane	9.48	0.92
2D ray-tracing	6.52	0.95
3D urban	5.89	0.96
<i>Calibration from all measurements</i>		
Vertical-Plane	7.54	0.93
2D ray-tracing	6.38	0.94
3D urban	5.57	0.95

A. Microcellular Configuration in Munich

The microcellular measurement test of COST 231 [9] is a common reference to evaluate the model capabilities. The measurement campaign was carried out by Mannesmann Mobilfunk GmbH in downtown Munich with a 13-m-high transmitter site in the middle of a square. The transmitting frequency is 947 MHz. The terrain is only represented by building contours and building heights. The altimetry is assumed to be constant. The measurement drive test is about 28 km long with one averaged measurement point about every 12 m. The path loss varies from 75 to 170 dB. Moreover, the transmitter–receiver distance varies from 90 to 1900 m.

The 3-D urban model and the 2-D ray-tracing model basically allow four successive reflections and one diffraction on the building vertical edges. The reflections after diffraction and the interactions with far obstacles are not allowed.

The three models under test are calibrated following two different processes. The first process is the “blind test” that was specified by COST 231. The models are calibrated from 11 path loss measurements only; then, the performance of the calibrated models is determined from comparison to all measurements. The second process consists of calibrating the models from all measurements. The results from both processes are presented in Table II. We observe in both cases the obvious efficiency of the 3-D urban model that reduces the RMS error by 2 dB compared with the vertical-plane model or by 0.8 dB compared with the 2-D ray-tracing model.

B. Delay-Spread From High-Tower Urban Transmitter

In this example, channel impulse responses were measured around a high-macrocell urban DVB transmitter with a directive panel antenna (60° half-power beamwidth). An 8-MHz-wide DVB signal is transmitted on channel 50, i.e., the central frequency is 706 MHz. The reception equipment is able to measure impulse responses with large power dynamics and is used here to characterize the wideband propagation channel [32].

The transmitter is located on top of a hill, illuminating a large part of a city, whereas the measurements are realized in 51 locations in the center of the town, as illustrated in Fig. 12. This configuration provides a large variety of impulse responses, which turned out to be challenging for the interpretation and evaluation of the propagation model.

Acquisitions of the impulse response are processed to get one averaged (out of 150 samples) PDP per location. The difference

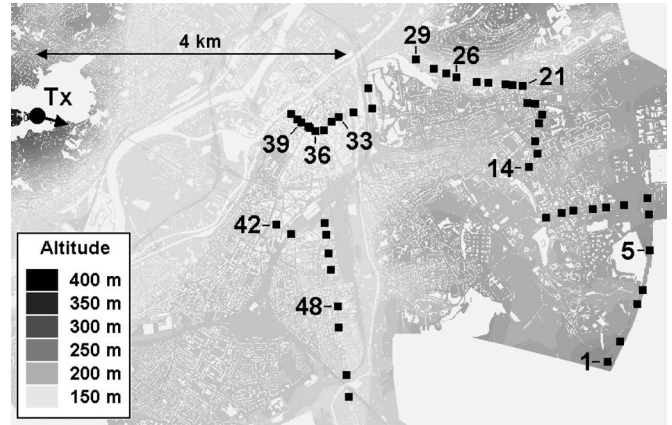


Fig. 12. Location of the transmitter and measurements. Figures are the index of the measurement locations.

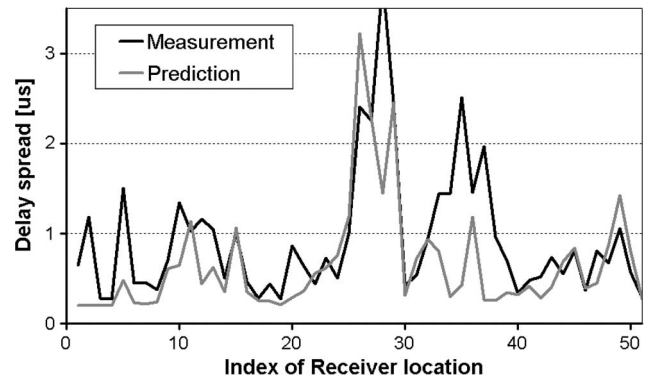


Fig. 13. Comparison between measured and predicted delay spreads.

between the peak power in the PDP and the noise floor is in the range from 44 to 56 dB. Excess delays of up to $11 \mu\text{s}$ are observed for significant contributions (power relative to the peak is greater than -15 dB), which means that strong far interactions (excess propagation path greater than 3.3 km) occur in this environment. Fig. 13 shows the delay spread measured at each location. The delay spread is only calculated from samples with power relative to the peak larger than -42 dB.

For simulation purposes, different receiver points are created along 30-m-long lines parallel to the street and centered on each measurement location. Predictions are realized at all these points with up to four reflections, one diffraction, and one far interaction allowed along one single ray. Delay spreads are computed following the same rule as for measurements. One averaged delay spread is calculated for each location. Fig. 13 shows that the prediction is able to find the main variations of delay-spread fluctuations with two exceptions. First, the prediction is pessimistic in locations from index 1 to 5. The reason is certainly that these locations are at the boundary of the HR geographical map data representing the city. Therefore, strong interactions with buildings beyond this boundary cannot be simulated. This stresses the importance of an accurate geographical map data to predict the wideband channel characteristics. Second, the prediction is pessimistic in locations from index 33 to 39 in the dense urban part of the city. The 3-D urban model simulates that there only

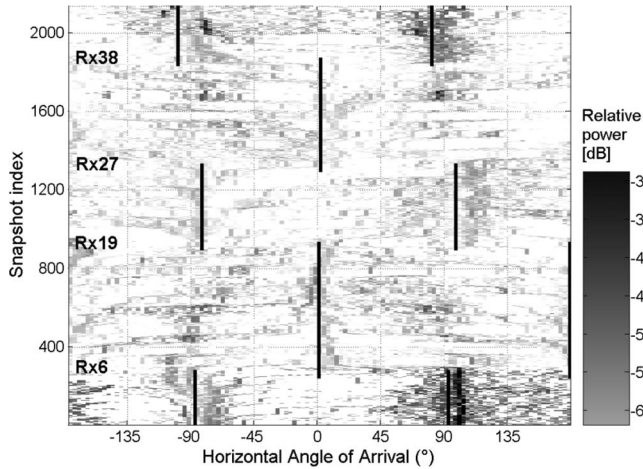


Fig. 14. Arrival azimuth power spectrum estimated by RIMAX.

a few contributions coming from distant interactions, as this kind of contribution is strongly attenuated by the dense urban environment surrounding the receiver. We assume that the measured delayed contributions are generated from a distant interaction and then from canyoning in the urban center, which has yet to be simulated. In addition, the ray tracing simulates a large number of rays with large delays for locations from index 25 to 29. These rays come from far reflections or diffractions on the buildings located on the hills surrounding the receiver. The prediction results are in good agreement with the measurements.

C. Angular-Spread From a Macrocell Suburban Transmitter

After evaluating the wideband performance of the 3-D urban model over large propagation distances, this last example compares the predictions of arrival angles to maximum likelihood parameter estimation framework (RIMAX) estimates in a small suburban macrocell, assessing the performance of the model for short propagation ranges. The measurement setup and the RIMAX estimates are presented in detail in [33]. Measurements were collected using a MIMO channel sounder with 120-MHz bandwidth at the central frequency 4.5 GHz. The fixed transmitter antenna is located 35 m above the ground, whereas the receiver antenna is on top of a car moving in a suburban area with typically two to three floor buildings. Some measurement portions are in LOS. Distances from the transmitter to the receiver are in the range from 130 to 380 m. The gradient-based maximum-likelihood estimation framework RIMAX was used to estimate both the angles and the delays of the specular multipath components. Fig. 14 presents the estimated arrival azimuth power along the route, where the power levels are normalized relative to the maximum global power. The index of the reference receiver locations ($R \times 6$, $R \times 19$, etc.) is reported in the figure to relate the results to the route description in [33]. The black vertical lines represent the orientation of the streets. Then, the contributions coming parallel or perpendicular to the street can be distinguished. Fig. 14 shows a high spatial dispersion of the channel from location $R \times 6$ to location $R \times 38$, where the direct path is strongly attenuated by building obstructions.

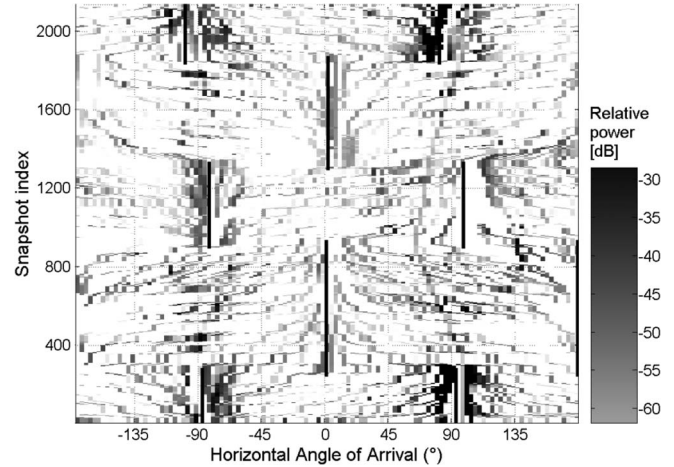


Fig. 15. Arrival azimuth power spectrum from predictions.

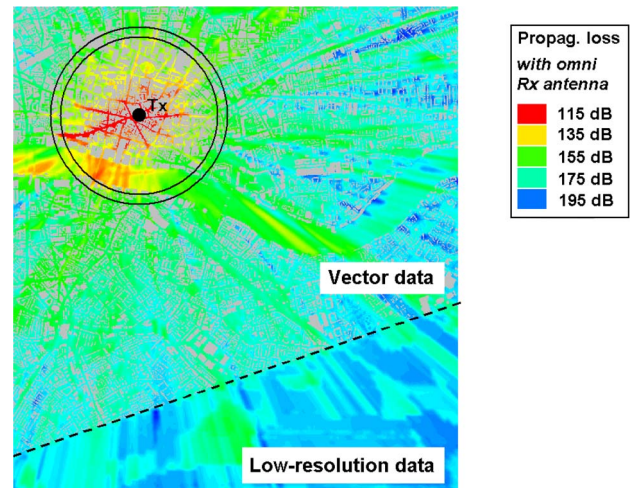


Fig. 16. Extract of the 16 km² coverage map.

The wideband propagation channel is predicted from the 3-D urban model that allows two reflections and one diffraction. The resulting arrival azimuth power is displayed in Fig. 15 for comparison. We observe that the main evolutions of the AoA predicted along the route are in good agreement with the RIMAX estimates.

V. COVERAGE RESULTS FOR PLANNING AND OPTIMIZATION

Fig. 16 presents a 5-m-resolution coverage map predicted around the same transmitter as in Section II. The limits of the near-reception and transition-reception regions are represented by black circles. The geographical map data are heterogeneous, as the south-east part contains LR raster data only. The 3-D urban model handles this heterogeneity by constructing the vertical terrain profiles with a mix of LR and HR data, as mentioned in Section IV. Wideband channel parameters are predicted in the near-reception region, like the horizontal arrival angle spread or the delay spread shown in Figs. 17 and 18. The computation times given in Table III are averaged values per sector, assuming a three-sector transmitter. The full 3-D urban prediction is done for the first sector. Then, other antenna

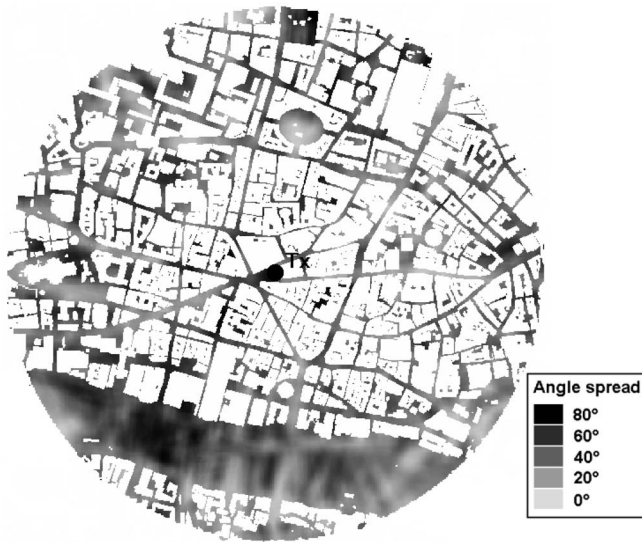


Fig. 17. Simulated map of the horizontal arrival angle spreads.

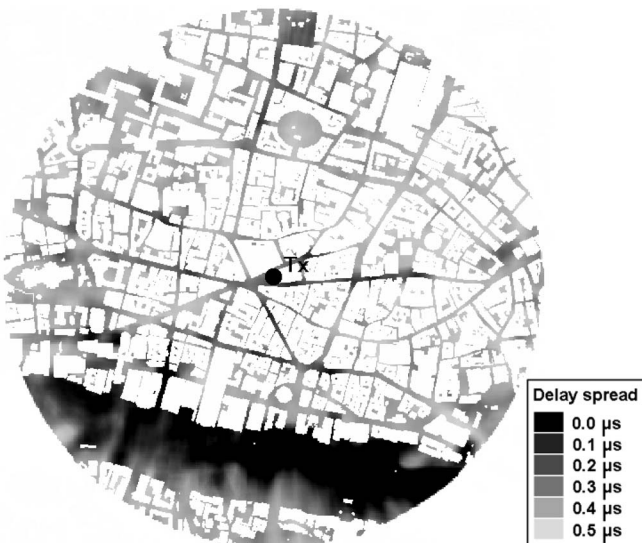


Fig. 18. Simulated map of the delay spreads.

TABLE III
AVERAGED COMPUTATION TIMES FOR A THREE-SECTOR
TRANSMITTER ON A PIII (2 GHz)

Model	Surface	Resolution	Time
4 Refl. – 1 Diffr.	64 km ²	5 m	400 s
2 Refl. – 1 Diffr.	64 km ²	5 m	310 s
2 Refl. – 1 Diffr.	16 km ²	5 m	60 s

tilts and azimuths are immediately predicted from successive antenna unmasking–masking operations.

These times are strongly dependent on the vector density and the transmitter configuration; thus, they cannot be generalized to any other setup. However, they prove that this kind of deterministic prediction can be introduced into the operational radio planning and optimization process with reasonable computation times.

VI. CONCLUSION

The planning and optimization of new wideband radio networks over large geographical areas with deterministic tools are two engineering tasks made possible by techniques such as those presented in the paper. The presented 3-D urban model is a fast and robust propagation model that gathers most of the advantages of the state-of-the-art methods. It efficiently computes 3-D ray contributions in any urban radio configuration by separating the analysis into a vertical plane and a horizontal plane. The ray-launching technique makes use of reflection and diffraction VMs to efficiently catch the useful rays. Furthermore, the separation into near- and far-reception regions and the support for multiresolution and heterogeneous geographical map data, coupled with an efficient software engineering, allow for the use of large operational network topologies. The model combines a fast and accurate multipath computation in dense urban areas and a large-scale estimation of the received field in surrounding areas. In addition, the possible unmasking and masking of the previously computed ray contributions for each location allow optimal use for network optimization tasks.

Another key advantage of the method is to be able to take into account hilly grounds in dense urban areas involving strong multipath.

The comparison with drive-test power measurements proves the robustness and accuracy of the 3-D urban model when predicting the narrowband power level in strong multipath environments. Many studies realized in the past few years indicate that, generally, the power prediction gets an error RMS in the range from 5 to 8 dB after tuning. Moreover, the comparison to impulse response measurements shows the ability to provide realistic wideband predictions. The delay spreads predicted at receivers located in a hilly city (which are a few kilometers away from the transmitter) are in good agreement with the measurements. In particular, large delay spreads are measured and predicted (from significant contributions having up to 11 μ s excess delay) in some obstructed locations.

This model is extensively used in many countries for radio planning and optimization computations nationwide and in challenging cities like New York City and Hong Kong. It is generally used for the calculation of coverage maps with a resolution of 5 m and a radius from 1 to 5 km. Most of the ray-tracing computation is restricted to the surroundings of the transmitter as the radius of the ray-tracing region is typically less than 1 km. Then, the average computation time is only on the order of 1 min per transmitter with a standard PC configuration.

The model also provides inputs for the site-specific tap-delay model used in system-level algorithms that aim to design new air interfaces.

The model is suitable for simulating statistics of the MIMO system capacity using the ray characteristics to estimate the relation between the distinct radio channels. Even if the exact phase of ray fields is unknown, the phase changes from one antenna element to another are calculated from the ray geometry.

Enhancements of the method are currently implemented to further optimize the performances, particularly for MIMO applications, taking into account the rich scattering environments. One solution is the deterministic construction of diffuse

scattering components from the building walls close the transmitter or the receiver [34]. Another solution, which is complementary to the previous solution, consists of the introduction of statistical components based on a macroscopic analysis of the propagation environment. A mix approach, which predicts the simplest specular contributions in a deterministic way and the other contributions in a statistical way, should be able to provide site-specific and realistic wideband channels.

REFERENCES

- [1] ITU, *Recommendation ITU-R M.1457-6—Detailed Specifications of the Radio Interfaces of International Mobile Telecommunications-2000 (IMT-2000)*, Dec. 2006. ITU Recommendation.
- [2] H. Holma and A. Toskala, *WCDMA for UMTS*. Hoboken, NJ: Wiley, 2001.
- [3] *Third Generation Partnership Project (3GPP)*. [Online]. Available: www.3gpp.org
- [4] *Third Generation Partnership Project 2 (3GPP2)*. [Online]. Available: www.3gpp2.org
- [5] *IEEE Standard for Local and Metropolitan Area Networks Part 16 (IEEE 802.16)*. [Online]. Available: <http://standards.ieee.org/getieee802/802.16.html>
- [6] *WiMAX Forum*. [Online]. Available: www.wimaxforum.org
- [7] *Digital Video Broadcasting Project (DVB)*. [Online]. Available: www.dvb.org
- [8] A. Schertz and C. Weck, "Hierarchical modulation—The transmission of two independent DVB-T multiplexes on a single frequency," *EBU Tech. Rev.*, Apr. 2003.
- [9] T. K. Sarkar, Z. Ji, K. Kim, A. Medouri, and M. Salazar-Palma, "A survey of various propagation models for mobile communication," *IEEE Antennas Propag. Mag.*, vol. 45, no. 3, pp. 51–82, Jun. 2003.
- [10] "Digital mobile radio towards future generation systems," *COST 231 Final Rep.*, 1999.
- [11] L. M. Correia, *Wireless Flexible Personalized Communications*. Hoboken, NJ: Wiley, 2001. COST 259 Final Rep.
- [12] L. M. Correia, "Mobile broadband multimedia networks," in *Report on the Research Work of COST 273*. New York: Academic, 2006.
- [13] K. Rizk, J.-F. Wagen, and F. Gardiol, "Ray tracing based path loss prediction in two microcellular environments," in *Proc. IEEE PIMRC*, Hague, The Netherlands, Sep. 1994, pp. 384–388.
- [14] S. Y. Tan and H. S. Tan, "Propagation model for microcellular communications applied to path loss measurements in Ottawa City streets," *IEEE Trans. Veh. Technol.*, vol. 44, no. 2, pp. 313–317, May 1995.
- [15] J. P. Rossi and Y. Gabillet, "A mixed ray launching/tracing method for full 3-D propagation modeling and comparison with wide-band measurements," *IEEE Trans. Antennas Propag.*, vol. 50, no. 4, pp. 517–523, Apr. 2002.
- [16] T. Fügen, J. Maurer, T. Kayser, and W. Wiesbeck, "Capability of 3-D ray tracing for defining parameter sets for the specification of future mobile communications systems," *IEEE Trans. Antennas Propag.*, vol. 54, no. 11, pp. 3125–3137, Nov. 2006.
- [17] J. Maurer, O. Drumm, D. L. Didascalou, and W. Wiesbeck, "Ray-density normalisation in the determination of visible surfaces in 3D vector geometries for ray-optical wave propagation modelling," in *Proc. 51st IEEE Veh. Technol. Conf.*, Tokyo, Japan, May 2000, pp. 1651–1655.
- [18] P. Combeau, R. Vauzelle, Y. Pousset, and L. Aveneau, "An optimization in computation time for the prediction of radio coverage zones," *Radio Sci.*, vol. 42, no. 1, p. RS1 003, 2007.
- [19] G. Liang and H. L. Bertoni, "A new approach to 3-D ray tracing for propagation prediction in cities," *IEEE Trans. Antennas Propag.*, vol. 46, no. 6, pp. 853–863, Jun. 1998.
- [20] T. Kürner and A. Meier, "Prediction of outdoor and outdoor-to-indoor coverage in urban areas at 1.8 GHz," *IEEE J. Sel. Areas Commun.*, vol. 20, no. 3, pp. 496–506, Apr. 2002.
- [21] T. Kürner, A. Eisenblaetter, H. F. Geerdes, D. Junglas, T. Koch, and A. Martin, "Final report on automatic planning and optimisation," *IST Momentum Project*, Oct. 2003.
- [22] J. Deygout, "Multiple knife diffraction of microwave," *IEEE Trans. Antennas Propag.*, vol. AP-14, no. 4, pp. 480–489, Jul. 1966.
- [23] Y. Corre, Y. Lostanlen, and Y. L. Helloco, "A new approach for radio propagation modeling in urban environment: Knife-edge diffraction combined with 2D ray-tracing," in *Proc. Veh. Technol. Conf.*, Birmingham, AL, May 2002, pp. 507–511.
- [24] J. Walfisch and H. L. Bertoni, "A theoretical model of UHF propagation in urban environments," *IEEE Trans. Antennas Propag.*, vol. 36, no. 12, pp. 1788–1796, Dec. 1988.
- [25] T. Kürner, D. J. Cichon, and W. Wiesbeck, "Concepts and results for 3D digital terrain-based wave propagation models: An overview," *IEEE J. Sel. Areas Commun.*, vol. 11, no. 7, pp. 1002–1012, Sep. 1993.
- [26] K. Rizk, R. Valenzuela, S. Fortune, D. Chizhik, and F. Gardiol, "Lateral, full-3D and vertical plane propagation in microcells and small cells," in *Proc. IEEE 48th Veh. Technol. Conf.*, Ottawa, ON, Canada, May 1998, vol. 2, pp. 998–1003.
- [27] A. S. Glassner, *An Introduction to Ray-Tracing*. San Mateo, CA: Morgan Kaufmann, 1989.
- [28] Y. Corre and Y. Lostanlen, "An enhanced method to extrapolate in 3D antenna radiation patterns in the context of the radio network planning," in *Proc. EUCAP*, Nice, France, Sep. 2006, p. 441.
- [29] W. D. Burnside and K. W. Burgener, "High frequency scattering by a thin lossless dielectric slab," *IEEE Trans. Antennas Propag.*, vol. AP-31, no. 1, pp. 104–110, Jan. 1983.
- [30] R. Luebbers, "A heuristic UTD slope diffraction coefficient for rough lossy wedges," *IEEE Trans. Antennas Propag.*, vol. 37, no. 2, pp. 206–211, Feb. 1989.
- [31] L. P. Ivriissimtzis and R. J. Marhefka, "A note on double edge diffraction for parallel wedges," *IEEE Trans. Antennas Propag.*, vol. 39, no. 10, pp. 1532–1537, Oct. 1991.
- [32] Y. Corre and Y. Lostanlen, "Parameter characterization of DVB wideband wireless systems," in *Proc. PIMRC, Multimedia Session*, Cannes, France, Sep. 2008.
- [33] M. Landmann, K. Sivasondhivat, J.-I. Takada, I. Ida, and R. Thomä, "Polarisation behaviour of discrete multipath and diffuse scattering in urban environments at 4.5 GHz," *EURASIP J. Wireless Commun. Netw.*, vol. 2007, no. 1, p. 60, Jan. 2007. Article ID 57980.
- [34] F. Fuschini, H. El-Sallabi, V. Degli-Esposti, L. Vuokko, D. Guiducci, and P. Vainikainen, "Analysis of multipath propagation in urban environment through multidimensional measurements and advanced ray tracing simulation," *IEEE Trans. Antennas Propag.*, vol. 56, no. 3, pp. 848–857, Mar. 2008.



R&D projects.



Yoann Corre received the Dipl.-Ing. degree from the National Institute for Applied Sciences, Rennes, France, and the M.Sc. degree from University College London, London, U.K., in 1999.

He is currently a Research and Development (R&D) Engineer with the Radio Department, Siradel, Rennes, where he is working on radio wave propagation applied to various domains such as radio communication systems and digital television. He was involved in the European IST-PLUTO project and many regional and national-level collaborative

Yves Lostanlen (S'98–M'01) received the Dipl.-Ing (M.Sc.) degree from the National Institute for Applied Sciences, Rennes, France. After three years of research at University College London, London, U.K., he received the European Ph.D. degree with highest honors.

He is currently the Vice President and the Wireless CTO in the wireless industry with Siradel, Rennes, dealing with radio channel modeling, communication system design, and network planning, optimization, and monitoring. He opened the Radio Expertise and Research Centre of Siradel in Toronto, ON, Canada, (including future wireless internet, 4G+, geolocation, and flexible radio) in January 2009.

Dr. Lostanlen regularly holds lectures, tutorials, seminars, workshops, and training sessions in industrial and academic institutions. He is engaged in leading standardization and academic bodies including the IEEE, the International Union of Radio Science (URSI), and COST2100.